Stochastic simulation of chemical exchange in two dimensional infrared spectroscopy

František Šanda[a)]
Department of Chemistry, University of California, Irvine, California 92697-2025 and Institute of Physics, Faculty of Mathematics and Physics, Charles University, Ke Karlovu 5, Prague 121 16, The Czech Republic

Shaul Mukamel[b)]
Department of Chemistry, University of California, Irvine, California 92697-2025

(Received 14 March 2006; accepted 24 April 2006; published online 6 July 2006)

The stochastic Liouville equations are employed to investigate the combined signatures of chemical exchange (two-state jump) and spectral diffusion (coupling to an overdamped Brownian oscillator) in the coherent response of an anharmonic vibration to three femtosecond infrared pulses. Simulations reproduce the main features recently observed in the OD stretch of phenol in benzene. © *2006 American Institute of Physics*. [DOI: 10.1063/1.2205367]

I. INTRODUCTION

Chemical exchange processes cause time-dependent spectral jumps between stable configurations of molecular complexes. These are accompanied by coherence transfer which has distinct spectroscopic signatures. NMR line shapes are commonly analyzed in terms of chemical exchange on the millisecond time scale.[1–4] As the exchange rate is increased the line shapes first broaden and become narrower for faster rates. This motional narrowing reflects an averaging of fluctuations. Recent experiments demonstrated that two dimensional infrared (2D IR) line shapes can probe the picosecond dynamics of chemical exchange by observing coherence transfer in molecular vibrations.[5–7]

The 2D IR spectrum is obtained using three pulses (Fig. 1).[8–10] The first pulse creates a vibrational coherence, whose evolution (free induction decay) during the first interval t_1 is related to the absorption line shape by a Fourier transform. During the second t_2 interval (population time) the vibrational frequency changes stochastically by complexation with the solvent. Finally vibrational coherence is again created by the third pulse and the signal is heterodyne detected after the third interval t_3. The correlations of the line shapes in the first and the third intervals provide information on chemical exchange processes which take place during the second interval.

Due to the spatial coherence in the optical response the signal is generated along phase-matching directions which correspond to the various Liouville space pathways of the vibrational density matrix. Certain combinations of these pathways[11,12] give absorptive 2D line shapes which are more clearly resolved. Chemical exchange dynamics is clearly seen by a two dimensional Fourier transform of the signals with respect to t_1 and t_3 and plotting them versus the conjugate frequencies ω_1 and ω_3 for various values of t_2.

A recent experiment[5] looked at the OD stretching mode of phenol in benzene whose frequency fluctuates between 2665 cm^{-1} (free) and 2631 cm^{-1} (complexed). The 2D line shapes monitored the dynamics of complex formation and dissociation.[5] For short delays ($t_2 \sim 100$ fs) two diagonal peaks broadened by spectral diffusion were observed at the linear-absorption frequencies for short delays. For longer times ($t_2 \sim 10$ ps) additional off-diagonal cross peaks were induced by chemical exchange. Similar effects were seen in the overtone region. The rate constants for complexation were directly measured from the peak kinetics.

Similar hydrogen-bonding dynamics was reported for the CN stretch of acetonitrile in methanol.[7] The relative intensity of the two peaks attributed to free and hydrogen-bonded CN shows strong temperature dependence. The reaction coordinate profile in both ground and excited vibrational states was found to be very similar.

The weak variation of the chemical-exchange rates with changes in the vibrational state justifies the application of stochastic chemical exchange models[13] for vibration frequency fluctuations. The stochastic Liouville equations (SLEs) describe the dynamics of a quantum system (vibrational coherence) perturbed by a stochastic process (chemical exchange and spectral diffusion) described by a Markovian master equation. This formalism was recently applied to model the signatures of conformational fluctuations in trialanine in water[17] using a Brownian oscillator coordinate model of fluctuations. The SLEs were also used to compare the Brownian oscillator and the four-state-jump model of hydrogen bonding fluctuation on the photon echo of the OH stretch of HOD in DOD.[18] In the present paper we use the SLE to simulate the effects of chemical exchange[14–16] and spectral diffusion in 2D line shapes of an anharmonic vibration. Our simulations reproduce all the effects observed recently[5] in the study of complexation dynamics of the OD stretch.

In Sec. II we introduce our model which consists of an anharmonic vibration subjected to fluctuations due to a two-state chemical exchange and a Brownian oscillator coordinate. Expressions for the 2D IR signals are given in Sec. III.

[a)]Electronic mail: sanda@karlov.mff.cuni.cz
[b)]Electronic mail: smukamel@uci.edu

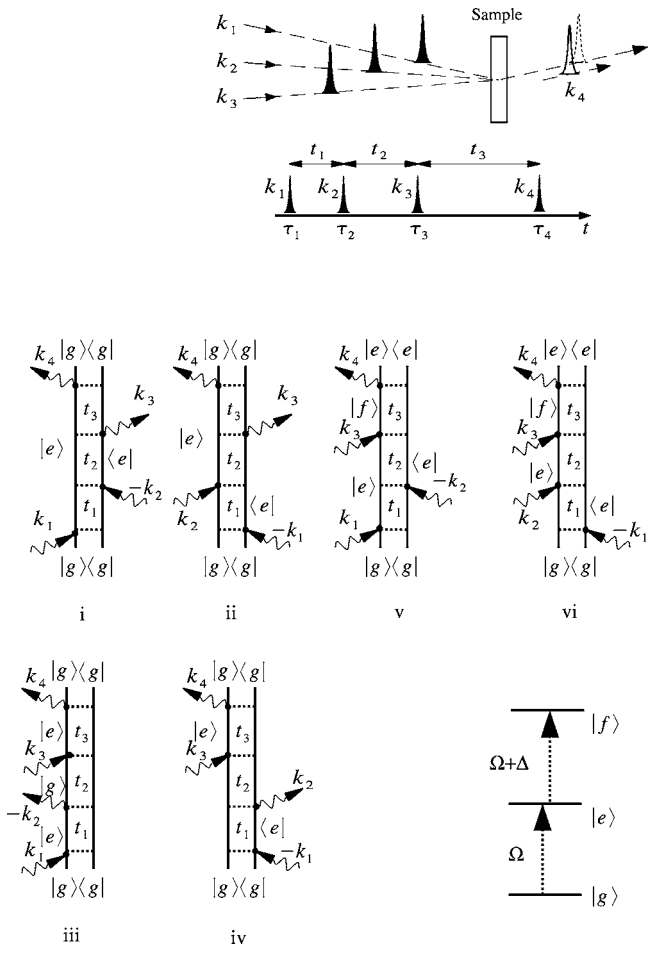

FIG. 1. Top: pulse configuration for a three pulse cohrent experiment. Bottom: Feynman diagrams for the third order coherent response of an anharmonic vibrations. The diagrams correspond, respectively, to the six terms in Eq. (6).

The stochastic Liouville equation for the two-state-jump (TSJ) model is introduced in Sec. IV. In the TSJ model of Kubo[4,19] and Anderson *et al.*[20] bath-assisted (incoherent) chemical exchange is described by kinetic equations.[21,22] The model shows several distinct dynamical regimes depending on the motional narrowing parameter (ratio of the frequency shift and relaxation rate) and the 2D IR signals are calculated for the limiting cases of slow and fast fluctuations and for short and long-time delays between pulses. Spectral diffusion is incorporated by coupling to an overdamped Brownian oscillator coordinate[23] in Sec. V. The combined effect of spectral diffusion and TSJ is presented and analyzed. All line shape regimes observed in Ref. 5 are reproduced.

II. THE MODEL

We consider a single anharmonic vibrational mode described by the Hamiltonian

$$H = \hbar\Omega B^\dagger B + \tfrac{1}{2}\hbar\Delta B^\dagger B^\dagger BB, \tag{1}$$

where $B^\dagger$ (B) are boson creation (annihilation) operators ($[B,B^\dagger]=1$). Both frequency (Ω) and anharmonicity (Δ) are subjected to fluctuations described by

$$\Omega = \Omega_0 + \Omega_1\sigma_z + \Omega_2 Q + \Omega_3\sigma_z Q,$$
$$\Delta = \Delta_0 + \Delta_1\sigma_z + \Delta_2 Q + \Delta_3\sigma_z Q. \tag{2}$$

Ω_0 and Δ_0 are the average values. Ω_1 and Δ_1 describe stochastic frequency modulation by chemical exchange represented by the TSJ model[19,20] [state up $u(\sigma_z=1)$ and down $d(\sigma_z=-1)$]. σ_z is the Pauli spin matrix,

$$\sigma_z = \begin{pmatrix} 1 & 0 \\ 0 & -1 \end{pmatrix},$$

Q is an overdamped Brownian oscillator coordinate, whose coupling to the vibration through the parameters Ω_2 and Δ_2 causes spectral diffusion. Ω_3 and Δ_3 allow the spectral diffusion to have a different magnitude in the two spin states.

We shall divide the Hamiltonian [Eq. (1)] into three parts $H=H_S+H_Q+H_{QS}$, where H_S includes the first two (spin +vibration) terms in Eq. (2) which do not depend on Q, and H_Q and H_{QS} include the third and fourth terms in Eq. (2), respectively. The dipole interaction with the electric field $E(t)$ is[24]

$$H_{\rm int} = -\mu E(t)(B^\dagger + B). \tag{3}$$

Three vibrational levels (Fig. 1) are accessible in a three-pulse experiment: the ground state $|g\rangle$, the first excited $|e\rangle \equiv B^\dagger|g\rangle$, and the doubly excited $|f\rangle \equiv (1/\sqrt{2})B^\dagger B^\dagger|g\rangle$ state. Their energies are 0, Ω, and $\Omega+\Delta$, respectively. The corresponding nine-component Liouville space basis set for the density matrix is denoted $|\nu\nu'\rangle\rangle \equiv |\nu\rangle\langle\nu'|$; $\nu,\nu' = e,f,g$. The dipole moment matrix elements are $\mu_{eg}=\mu$ and $\mu_{ef}=\sqrt{2}\mu$.

III. THE THIRD ORDER RESPONSE AND 2D SIGNALS

We consider an impulsive four wave mixing process whereby the electric field [Eq. (1)] consists of three impulsive optical pulses with intervals t_1, t_2, and calculate the response at t_3 (see Fig. 1). Interactions with the field can create or annihilate one vibrational quantum at a time [Eq. (3)]. The equilibrium distribution is

$$|\rho(0)\rangle\rangle_{\mathcal{H}} = |\rho(0)\rangle\rangle_S |0\rangle_Q |gg\rangle, \tag{4}$$

where $|\rho(0)\rangle\rangle_S$ represents the spin state and $|0\rangle_Q$ [Eq. (3)] represents the Brownian coordinate. The space $\mathcal{H}$ is a direct product of the vibrational, spin, and the Brownian oscillator space.

The polarization generated in this experiment is described by the third order response function,[8]

$$S^{(3)}(t_1,t_2,t_3) = \left(\frac{i}{\hbar}\right)^3 \theta(t_1)\theta(t_2)\theta(t_3) \times \langle\langle I|\mu^{(-)}\mathcal{G}(t_3)\mu^{(-)}\mathcal{G}(t_2)\mu^{(-)}\mathcal{G}(t_1)\mu^{(-)}|\rho(0)\rangle\rangle_{\mathcal{H}}, \tag{5}$$

where $\mu^{(-)}\xi \equiv \mu[B+B^\dagger,\xi]$ (ξ is an arbitrary Hilbert space operator). Summing over final states is represented by $\langle\langle I|_{\mathcal{H}} \equiv \langle I|_S\langle 0|_Q$ Tr, where $\langle I|_S \equiv (1,1)$, $\langle 0|_Q \equiv \int dQ$, and the trace is over the vibrational degrees of freedom $\mathrm{Tr}=\langle\langle gg| + \langle\langle ee| + \langle\langle ff|$. The time evolution between pulses is described by

Green's function $\mathcal{G}(t)$ of the SLE in the space $\mathcal{H}$.

The vibrational state cannot change between pulses, so that the Green's functions are block diagonal and the response functions can be separated into six contributions from different Liouville space pathways.

$$\begin{aligned}
R_i(t_3,t_2,t_1) &\equiv \langle I|\mathcal{G}_{eg,eg}(t_3)\mathcal{G}_{ee,ee}(t_2)\mathcal{G}_{eg,eg}(t_1)|\rho(0)\rangle_{QS},\\
R_{ii}(t_3,t_2,t_1) &\equiv \langle I|\mathcal{G}_{eg,eg}(t_3)\mathcal{G}_{ee,ee}(t_2)\mathcal{G}_{ge,ge}(t_1)|\rho(0)\rangle_{QS},\\
R_{iii}(t_3,t_2,t_1) &\equiv \langle I|\mathcal{G}_{eg,eg}(t_3)\mathcal{G}_{gg,gg}(t_2)\mathcal{G}_{eg,eg}(t_1)|\rho(0)\rangle_{QS},\\
R_{iv}(t_3,t_2,t_1) &\equiv \langle I|\mathcal{G}_{eg,eg}(t_3)\mathcal{G}_{gg,gg}(t_2)\mathcal{G}_{ge,ge}(t_1)|\rho(0)\rangle_{QS},\\
R_v(t_3,t_2,t_1) &\equiv \langle I|\mathcal{G}_{fe,fe}(t_3)\mathcal{G}_{ee,ee}(t_2)\mathcal{G}_{eg,eg}(t_1)|\rho(0)\rangle_{QS},\\
R_{vi}(t_3,t_2,t_1) &\equiv \langle I|\mathcal{G}_{fe,fe}(t_3)\mathcal{G}_{ee,ee}(t_2)\mathcal{G}_{ge,ge}(t_1)|\rho(0)\rangle_{QS},
\end{aligned} \tag{6}$$

These may be graphically represented by the Feynman diagrams given in Fig. 1. For the stochastic models of frequency fluctuations considered here we have $R_i=R_{iii}$ and $R_{ii}=R_{iv}$, so that we only need to consider four independent pathways.[25] Green's function matrix elements $\mathcal{G}_{fe,fe}(t_3)$, etc., are now matrices in the joint spin and Brownian oscillator space.

We shall display the signal using the mixed time-frequency representation,

$$R_\alpha(\omega_3,t_2,\omega_1) \equiv \int_0^\infty \int_0^\infty \exp(i\omega_1 t_1 + i\omega_3 t_3) R_\alpha(t_3,t_2,t_1) dt_3 dt_1, \tag{7}$$

Eq. (6) then reads

$$R_i(\omega_3,t_2,\omega_1) = \langle I|\mathcal{G}_{eg,eg}(\omega_3)\mathcal{G}_{ee,ee}(t_2)\mathcal{G}_{eg,eg}(\omega_1)|\rho(0)\rangle_{QS},$$

and similarly for other pathways, where

$$\mathcal{G}(\omega) \equiv \int_0^\infty \mathcal{G}(t) e^{i\omega t} dt$$

is the Green's function in the frequency domain.

We consider the coherent nonlinear signals generated in the $\mathbf{k}_\mathrm{I}=-\mathbf{k}_1+\mathbf{k}_2+\mathbf{k}_3$ and $\mathbf{k}_\mathrm{II}=\mathbf{k}_1-\mathbf{k}_2+\mathbf{k}_3$ phase-matching directions. Invoking the rotating wave approximation the $\mathbf{k}_\mathrm{I}$ (photon echo) signal is[25]

$$\begin{aligned}
S_\mathrm{I}(\omega_3,t_2,\omega_1) = \left(\frac{i}{\hbar}\right)^3 \{&\mu_{eg}^4 [R_{ii}(\omega_3,t_2,\omega_1) + R_{iv}(\omega_3,t_2,\omega_1)]\\
&+ \mu_{eg}^2 \mu_{ef}^2 R_{vi}(\omega_3,t_2,\omega_1)\},
\end{aligned} \tag{8}$$

and for the $\mathbf{k}_\mathrm{II}$ signal we have

$$\begin{aligned}
S_\mathrm{II}(\omega_3,t_2,\omega_1) = \left(\frac{i}{\hbar}\right)^3 \{&\mu_{eg}^4 [R_i(\omega_3,t_2,\omega_1) + R_{iii}(\omega_3,t_2,\omega_1)]\\
&+ \mu_{eg}^2 \mu_{ef}^2 R_v(\omega_3,t_2,\omega_1)\}.
\end{aligned} \tag{9}$$

We shall also display the following combination of the two signals which shows absorptive peaks:[11,12]

$$S_A(\omega_3,t_2,\omega_1) \equiv -\mathrm{Im}[S_\mathrm{I}(\omega_3,t_2,-\omega_1) + S_\mathrm{II}(\omega_3,t_2,\omega_1)]. \tag{10}$$

When during the interval t_3 the system has no memory about its state in t_1, the third order response functions are factorized into products of the linear response functions $K(t)$,

$$\begin{aligned}
R_{iii}(t_3,t_2,t_1) &= K(t_3)K(t_1),\\
R_{iv}(t_3,t_2,t_1) &= K(t_3)K^*(t_1),\\
R_{iv}(\omega_3,t_2,\omega_1) &= K(\omega_3)K^*(-\omega_1).
\end{aligned} \tag{11}$$

For the stochastic model R_i and R_{ii} are factorized in the same way. Neglecting the overtone contributions R_v and R_{vi} it follows that the S_A signal is given by the product of the linear absorption line shapes W_A [Eq. (A1)],

$$\hbar S_A(\omega_3,\omega_1) = W_A(\omega_1)W_A(\omega_3). \tag{12}$$

IV. STOCHASTIC LIOUVILLE EQUATIONS FOR THE TWO-STATE-JUMP MODEL

The stochastic Liouville equations[13,26] are constructed by combining the Liouville equation, the dynamics of a quantum coherence, and a Markovian master equation describing a stochastic process,

$$\frac{d\rho}{dt} = \hat{\mathcal{L}}\rho(t) = \frac{-i}{\hbar}[H,\rho(t)] + \hat{L}\rho(t). \tag{13}$$

Stochastic models are closely related to microscopic models of bath variables.[8,23] Their optical response corresponds to the real part of the microscopic line broadening function[8] [see also Eq. (C6)]. Due to the fluctuation-dissipation theorem, the real part dominates at high temperatures, where the stochastic model becomes exact. (Limitations are discussed below.)

We first focus on the TSJ model[4,19,20] by neglecting the spectral diffusion (setting Δ_2, Δ_3, Ω_2, $\Omega_3=0$). The total density matrix ρ has 18 components $|\nu\nu' s\rangle\rangle$ given by the direct product of nine Liouville space states $|\nu\nu'\rangle\rangle$ and the two spin states, $s=u,d$. The Liouville operator $\hat{\mathcal{L}}$ is diagonal in the vibrational Liouville space variables, and is thus given by nine 2×2 diagonal blocks in spin space,

$$[\hat{\mathcal{L}}]_{\nu\nu' s,\nu_1\nu_1' s'} = \delta_{\nu\nu_1}\delta_{\nu'\nu_1'}[\hat{L}_S]_{s,s'} + \delta_{\nu\nu_1}\delta_{\nu'\nu_1'}\delta_{ss'}[\hat{\mathcal{L}}_S]_{\nu\nu' s,\nu\nu' s}, \tag{14}$$

where $\hat{L}_S$ describes the two-state-jump kinetics and $\hat{\mathcal{L}}_S$ represents the coherent vibrational evolution that depends parametrically on the spin state.

Chemical exchange is described by the rate matrix $\hat{\mathcal{L}}_S$ for the spin,

$$[\hat{L}_S] = \begin{pmatrix} -k_d & k_u \\ k_d & -k_u \end{pmatrix}. \tag{15}$$

The up (down) jump rates $k_u(k_d)$ are connected by the detailed-balance relation $k_u/k_d=\exp\beta(\epsilon_d-\epsilon_u)$, where $\epsilon_d-\epsilon_u$ is the energy difference between the u and d states.

The equilibrium density matrix is

$$|\rho(0)\rangle\rangle = |gg\rangle\rangle|\rho(0)\rangle_S, \quad |\rho(0)\rangle_S = \frac{1}{k_u + k_d}\begin{pmatrix} k_u \\ k_d \end{pmatrix}. \tag{16}$$

We next turn to the coherent part $\hat{\mathcal{L}}_S \equiv -(i/\hbar)[H_S, \ldots]$. For the $|gg\rangle\rangle$, $|ee\rangle\rangle$, and $|ff\rangle\rangle$ blocks, $[\hat{\mathcal{L}}_S]_{gg,gg} = [\hat{\mathcal{L}}_S]_{ee,ee} = [\hat{\mathcal{L}}_S]_{ff,ff} = 0$. The other blocks of $\mathcal{L}_S$ are

$$[\hat{\mathcal{L}}_S]_{eg,eg} = \begin{pmatrix} -i(\Omega_0 + \Omega_1) & 0 \\ 0 & -i(\Omega_0 - \Omega_1) \end{pmatrix},$$

$$[\hat{\mathcal{L}}_S]_{fe,fe} = \begin{pmatrix} -i(\Omega_0 + \Delta_0) - i(\Omega_1 + \Delta_1) & 0 \\ 0 & -i(\Omega_0 + \Delta_0) + i(\Omega_1 + \Delta_1) \end{pmatrix},$$

$$[\hat{\mathcal{L}}_S]_{fg,fg} = \begin{pmatrix} -i(2\Omega_0 + \Delta_0) - i(2\Omega_1 + \Delta_1) & 0 \\ 0 & -i(2\Omega_0 + \Delta_0) + i(2\Omega_1 + \Delta_1) \end{pmatrix}.$$

The remaining blocks are obtained by taking complex conjugates $[\hat{\mathcal{L}}_S]_{\nu\nu',\nu\nu'} = [\hat{\mathcal{L}}_S]^*_{\nu'\nu,\nu'\nu}$

These matrices may be represented in a compact form by defining the energy $\hbar\epsilon_0$ and splitting $\hbar\epsilon_1$ parameters $\epsilon_0^{(g)} = 0$, $\epsilon_0^{(e)} = \Omega_0$, $\epsilon_0^{(f)} = 2\Omega_0 + \Delta_0$, $\epsilon_1^{(g)} = 0$, $\epsilon_1^{(e)} = \Omega_1$, and $\epsilon_1^{(f)} = 2\Omega_1 + \Delta_1$. We then have

$$[\hat{\mathcal{L}}_S]_{\nu\nu',\nu_1\nu_1'} = \delta_{\nu\nu_1}\delta_{\nu'\nu_1'}\begin{pmatrix} -i(\epsilon_0^{(\nu)} - \epsilon_0^{(\nu')}) - i(\epsilon_1^{(\nu)} - \epsilon_1^{(\nu')}) & 0 \\ 0 & -i(\epsilon_0^{(\nu)} - \epsilon_0^{(\nu')}) + i(\epsilon_1^{(\nu)} - \epsilon_1^{(\nu')}) \end{pmatrix}. \tag{17}$$

The Green's function solution of Eq. (13) is given by 2×2 blocks for each vibrational state $|\nu\nu'\rangle\rangle$ of the density matrix,

$$[\mathcal{G}]_{\nu\nu',\nu_1\nu_1'}(t) \equiv [\exp(\hat{\mathcal{L}}t)]_{\nu\nu',\nu_1\nu_1'} = \delta_{\nu\nu_1}\delta_{\nu'\nu_1'} \times \left\{ \left(\frac{\eta_2}{\eta_2 - \eta_1}\hat{1} - \frac{1}{\eta_2 - \eta_1}\hat{\mathcal{L}}_{\nu\nu',\nu\nu'} \right) \exp(\eta_1 t) + \left(\frac{\eta_1}{\eta_1 - \eta_2}\hat{1} - \frac{1}{\eta_1 - \eta_2}\hat{\mathcal{L}}_{\nu\nu',\nu\nu'} \right) \exp(\eta_2 t) \right\}, \tag{18}$$

where η_j are the eigenvalues of each block of $\hat{\mathcal{L}}$,

$$\eta_1 = -\frac{k_d + k_u}{2} - i(\epsilon_0^{(\nu)} - \epsilon_0^{(\nu')}) + \sqrt{\frac{(k_d + k_u)^2}{4} - (\epsilon_1^{(\nu)} - \epsilon_1^{(\nu')})^2 + i(\epsilon_1^{(\nu)} - \epsilon_1^{(\nu')})(k_d - k_u)},$$

$$\eta_2 = -\frac{k_d + k_u}{2} - i(\epsilon_0^{(\nu)} - \epsilon_0^{(\nu')}) - \sqrt{\frac{(k_d + k_u)^2}{4} - (\epsilon_1^{(\nu)} - \epsilon_1^{(\nu')})^2 + i(\epsilon_1^{(\nu)} - \epsilon_1^{(\nu')})(k_d - k_u)}.$$

For the gg, ee, and ff spaces $\hat{\mathcal{L}}_S = 0$, and Eq. (18) reads

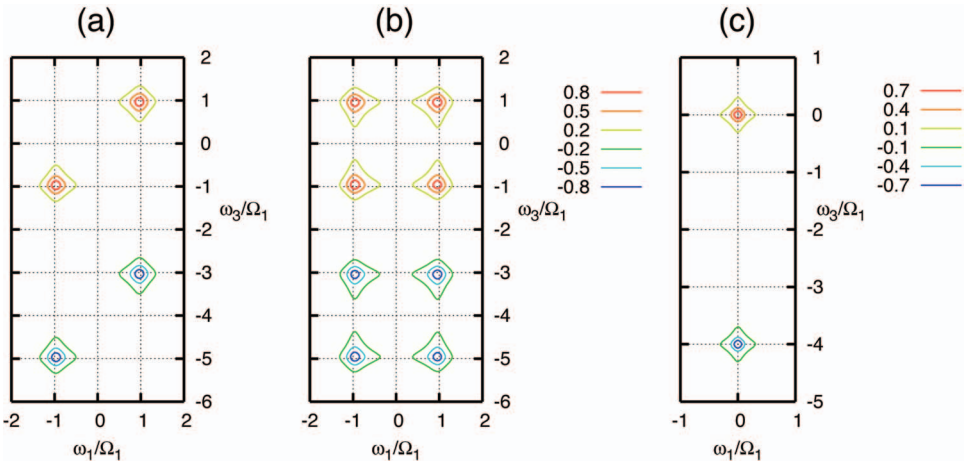

FIG. 2. (Color) 2D signals S_A [Eq. (10)] for the TSJ model [Eqs. (14) and (10)]: (a) static limit $\Omega_1/k_u = 5$ for short delay $k_u t_2 = 0$, $\Delta_0 = -4\Omega_1$, $k_d = k_u$, and $\Delta_1 = 0$, (b) static limit $\Omega_1/k_u = 5$ for long delay $k_u t_2 = 2.0$, $\Delta_0 = -4\Omega_1$, $k_d = k_u$, and $\Delta_1 = 0$, (c) fast chemical exchange (motional narrowing) $\Omega_1/k_u = 0.2$, $\Delta_0 = -4\Omega_1$, $\Delta_1 = 0$, $k_d = k_u$, and $k_u t_2 = 0$.

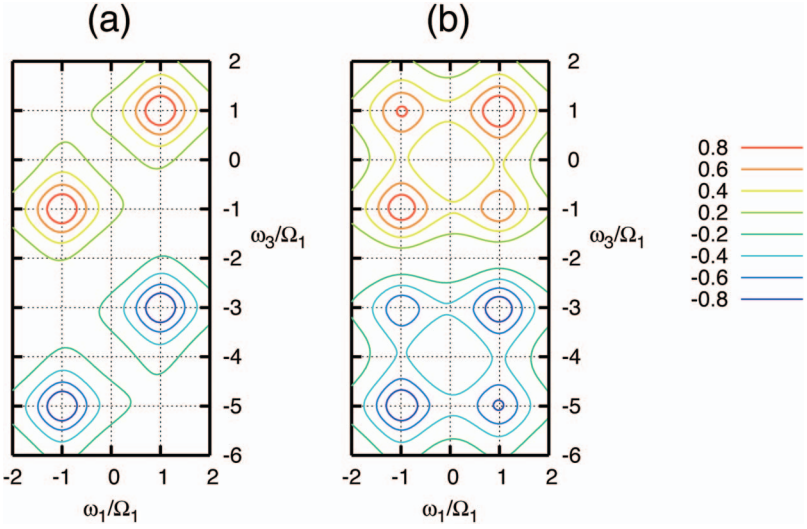

FIG. 3. (Color) The 2D signal S_A signal [Eq. (10)] including TSJ and the fast spectral diffusion: $\Omega_2/\Lambda=0.2$; $\Omega_2/\Omega_1=3$, and $k_d=k_u=0.002\Omega_1$; $\Delta_0=-4\Omega_1$, and $\Omega_3=\Delta_3=\Delta_1=\Delta_2=0$; (a) $k_dt_2=0$ and (b) $k_dt_2=1$.

$$\mathcal{G}_{ee,ee}(t)=\mathcal{G}_{gg,gg}(t)=\mathcal{G}_{ff,ff}(t)\equiv\exp(\hat{L}_S t)=\hat{1}+\frac{1-\exp[-(k_d+k_u)t]}{k_d+k_u}\begin{pmatrix}-k_d & k_u\\ k_d & -k_u\end{pmatrix}. \tag{19}$$

The linear response is given in Appendix A. Closed expressions for the various pathways are given in Appendix B. Below we discuss the 2D signals for limiting cases.

Figures 2(a) and 2(b) show the 2D signals S_A [Eq. (10)] in the slow bath limit $\Omega_1 \gg k$ ($k\equiv k_d=k_u$) where no spin jumps occur during the t_1 and t_3 intervals. In all figures we shift frequencies by setting $\Omega_0=0$ and normalize the signal to have maximum absolute value of 1. For $kt_2 \ll 1$ no spin jumps occur during the t_2 interval and we only see four peaks [Fig. 2(a)], two diagonal at $\omega_1=\omega_3=\Omega_0\pm\Omega_1$, and two overtones at $(\omega_1,\omega_3)=(\Omega_0+\Omega_1,\Omega_0+\Delta_0+\Omega_1+\Delta_1)$ and $(\Omega_0-\Omega_1,\Omega_0+\Delta_0-\Omega_1-\Delta_1)$. In the opposite $kt_2 \gg 1$ limit we see eight peaks [Fig. 2(b)]. The additional four cross peaks at $(\omega_1,\omega_3)=(\Omega_0+\Delta_0,\Omega_0-\Delta_0)$, $(\Omega_0-\Delta_0,\Omega_0+\Delta_0)$, $(\Omega_0-\Omega_1,\Omega_0+\Delta_0+\Omega_1+\Delta_0)$, and $(\Omega_0+\Omega_1,\Omega_0-\Omega_1+\Delta_0-\Delta_1)$ are induced by the spin jumps. Diagrams *i*, *ii*, *iii*, and *iv* in Fig. 1 describe the $g-e$ peaks at $\omega_1,\omega_3\sim\Omega$. Diagrams *v* and *vi* show the $e-f$ peaks at $\omega_1\sim\Omega+\Delta$.

Note that the relation [Eq. (B5)], similar to Eq. (12), is valid for individual peaks in the short time regime since peak shapes are not connected with any inhomogenity which carries memory. However, Eq. (12) does not apply for the entire 2D line shape, since the memory of spin state erases the cross peaks. In contrast, for long t_2 [Fig. 2(b)] this memory is lost and Eq. (12) applies (apart from the the overtone contributions).

In Fig. 2(c) we display S_A [Eq. (10)] in the fast k_u, $k_d \gg \Omega_1$ limit. We see a fundamental peak at $\omega_1=\omega_3=\Omega_0$ and an overtone at $\omega_1=\Omega_1$ and $\omega_3=\Omega_0+\Delta_0$. Linear response in the fast regime shows one peak (motional narrowing[19]). Any memory of the t_1 interval is lost in the t_3 interval and the factorization [Eq. (11)] holds resulting in Eq. (12) as observed in Fig. 2(c).

V. TWO-STATE JUMP WITH SPECTRAL DIFFUSION

Spectral diffusion is described by a dimensionless overdamped Brownian oscillator coordinate Q [Eq. (1)] with unit variance whose dynamics is given by the Fokker-Planck operator,[27]

$$L_Q=\Lambda\frac{\partial}{\partial Q}\left(Q+\frac{\partial}{\partial Q}\right), \tag{20}$$

where Λ is the relaxation rate. For fast fluctuations $\Omega_2/\Lambda \ll 1$, spectral diffusion may be accounted for by simply adding dephasing rates Ω_2^2/Λ to the line shapes. However, the

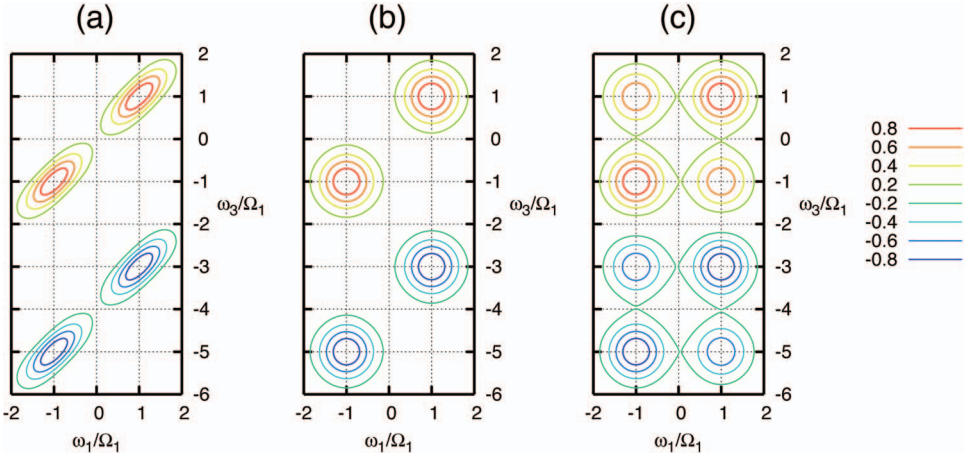

FIG. 4. (Color) The 2D S_A signal [Eqs. (10)] with TSJ and slow spectral diffusion: $\Omega_2/\Lambda=5$, $\Omega_2/\Omega_1=0.5$, $k_d=k_u=0.002\Omega_1$, $\Delta_0=-4\Omega_1$, $\Omega_3=\Delta_3=\Delta_2=\Delta_1=0$. (a) $\Lambda t_2=0$, (b) $\Lambda t_2=5$ (i.e., $k_dt_2=0.1$), and (c) $k_dt_2=1$.

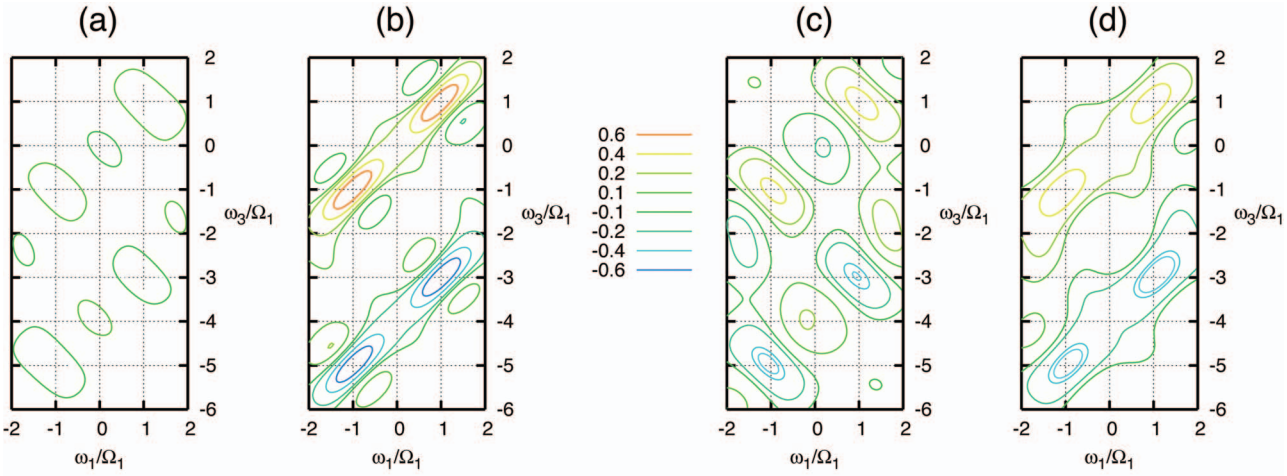

FIG. 5. (Color) 2D signals for S_{I} generated along $\mathbf{k}_{\mathrm{I}}$ [Eq. (8)], and S_{II} generated along $\mathbf{k}_{\mathrm{II}}$ [Eq. (9)]; (a) k_{II} and $\Lambda t_2=0$, (b) k_{I} and $\Lambda t_2=0$, (c) k_{II} and $\Lambda t_2=5$, and (d) k_{I} and $\Lambda t_2=5$. Other parameters same as in Fig. 4.

complete solution of the Fokker-Planck equation is required for arbitrary fluctuation time scales.

We define $\epsilon_2^{(g)}=0$, $\epsilon_2^{(e)}=\Omega_2$, and $\epsilon_2^{(f)}=2\Omega_2+\Delta_2$, and $\epsilon_3^{(g)}=0$, $\epsilon_3^{(e)}=\Omega_3$, and $\epsilon_3^{(f)}=2\Omega_3+\Delta_3$. The coupling of Q to the vibration is given by the Liouville operator $\hat{\mathcal{L}}_Q$,

$$[\hat{\mathcal{L}}_Q]_{\nu\nu' s,\nu_1\nu_1' s_1}=-i(\epsilon_2^{(\nu)}-\epsilon_2^{(\nu')})Q\delta_{\nu\nu_1}\delta_{\nu'\nu_1'}\delta_{ss_1},$$
$$[\hat{\mathcal{L}}_{QS}]_{\nu\nu' s,\nu_1\nu_1' s_1}=-i(\epsilon_3^{(\nu)}-\epsilon_3^{(\nu')})Q\delta_{\nu\nu_1}\delta_{\nu'\nu_1'}[\sigma_z]_{ss_1}. \tag{21}$$

The complete Liouville superoperator describing both TSJ and Brownian oscillator fluctuations is given by

$$\hat{\mathcal{L}}_{\mathrm{tot}}=\hat{L}_S+\hat{\mathcal{L}}_S+\hat{\mathcal{L}}_Q+\hat{\mathcal{L}}_{QS}+L_Q, \tag{22}$$

where $\hat{L}_S$ is given by Eq. (15), $\hat{\mathcal{L}}_S$ by Eq. (17), $\hat{\mathcal{L}}_Q$ and $\hat{\mathcal{L}}_{QS}$ by Eqs. (21), and L_Q by Eq. (20).

The response function for the spectral diffusion model alone[28] (neglecting the spin, setting $\Omega_1=0$, $\Delta_1=0$) can be calculated using the second order cumulant expansion[25] and is given in Appendix C.

We next turn to the third order response [Eq. (6)]. The equilibrium distribution is

$$|\rho(0)\rangle_{QS}=|\rho(0)\rangle_S|0\rangle_Q, \tag{23}$$

where $|\rho(0)\rangle_S$ is given by Eq. (16) and $|0\rangle_Q$ by Eq. (D1) and the final averaging should run over all degrees of freedom.

$$\langle I|_{QS}=\langle I|_S\langle 0|_Q.$$

The Green's function matrix elements $\mathcal{G}_{fe,fe}(t_3)$ are now matrices in the joint spin and Brownian oscillator space,

$$\mathcal{G}_{\nu\nu',\nu_1\nu_1'}(\omega)=-([i\omega+\hat{\mathcal{L}}_{\mathrm{tot}}]_{\nu\nu',\nu_1\nu_1'})^{-1}. \tag{24}$$

$\mathcal{G}(\omega_1)$ and $\mathcal{G}(\omega_3)$ are calculated in Appendix E by expanding them in the Fokker-Planck eigenmodes.[17,18,27,29]

During t_2 the evolution is in the ee, gg, and ff spaces where $\hat{\mathcal{L}}_{QS}=0$ and the Green's function may be factorized as

$$\mathcal{G}_{ee,ee}(t_2)=\mathcal{G}_{gg,gg}(t_2)=\exp(\hat{L}_S t_2)\exp(L_Q t_2). \tag{25}$$

The first factor is given by Eq. (19) and the second is the propagator of Fokker-Planck equation[27] expanded in its eigenmodes [Eq. (D1)],

$$[\exp(L_Q t)]_{\alpha\beta}=\delta_{\alpha\beta}\exp(-\alpha\Lambda t). \tag{26}$$

For slow chemical exchange (compared to the spectral diffusion k_u, $k_d \ll \sigma$, Λ) the TSJ peaks are well resolved and their line shapes are determined by the spectral diffusion. Chemi-

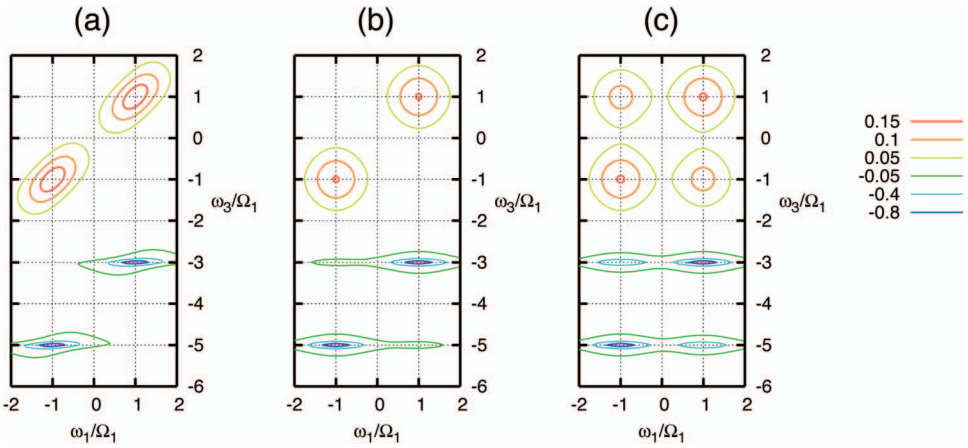

FIG. 6. (Color) 2D signal S_A [Eq. (10)] with spectral diffusion and TSJ. Spectral diffusion linewidth is varied ($\Delta_2\neq 0$). Slow spectral diffusion in eg state and fast diffusion in overtone ef: $\Omega_2/\Lambda=2$, $\Omega_2/\Omega_1=0.6$, $k_d=k_u=0.002\Omega_1$, $\Delta_0=-4\Omega_1$, $\Delta_2=-0.75\Omega_2$, $\Omega_3=\Delta_3=\Delta_1=0$. (a) $\Lambda t_2=0$, (b) $\Lambda t_2=15$ (i.e., $k_d t_2=0.1$), and (c) $k_d t_2=1$.

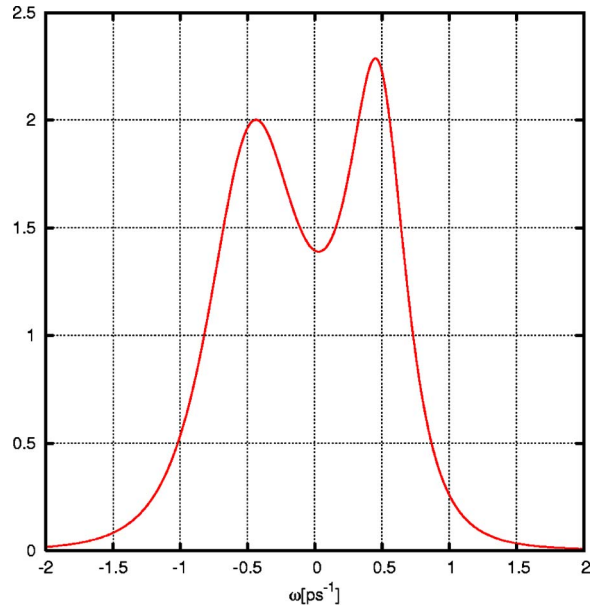

FIG. 7. (Color online) Absorption line shape for our model Eq. (22) with different spectral diffusion widths in the u and d states ($\Omega_3 \neq 0$). $\Omega_1 = 0.5\ \mathrm{fs}^{-1}$ $\Lambda = 0.4\ \mathrm{ps}^{-1}$, $\Omega_2 = 0.33\ \mathrm{ps}^{-1}$, $\Omega_3 = -0.07\ \mathrm{ps}^{-1}$, $k_d = 0.125\ \mathrm{ps}^{-1}$, $k_u = 0.1\ \mathrm{ps}^{-1}$, $\Delta_0 = -2.0\ \mathrm{ps}^{-1}$, $\Delta_2 = 0$, and $\Delta_3 = \Delta_1 = 0$.

cal exchange occurs on a much longer time scale and affects the cross peaks.

We start by setting Ω_3 and Δ_3 to 0 and examine fast and the slow spectral diffusion. The fast (motional narrowing) limit ($\Lambda \gg \Omega_2$) gives a Lorentzian absorption line shape. Since the bath has no memory, peak shapes are less sensitive to t_2 and cross peaks due to chemical exchange only appear as t_2 is increased. Effects of fast fluctuations may be accounted for by adding dephasing rates Ω_2^2/Λ. 2D line shapes S_A [Eq. (10)] shown in Fig. 3 are similar to the TSJ model (Fig. 2); both are given by a product of Lorentzian line shapes (in ω_1 and ω_3). The important difference is that for fast spectral diffusion, the linewidth is determined by both exchange and dephasing rates $(k_d + \Omega_2^2/\Lambda)^{-1}$, i.e., it is different from the cross-peak time scale. In contrast the linewidth of the TSJ model must be equal to the exchange rate k obtained by the growth rate of the cross peaks.

S_A in the static $\Lambda \ll \Omega_2$ limit (Fig. 4) shows Gaussian linear line shapes. Static disorder is eliminated in the photon echo $\mathbf{k}_\mathrm{I}$ experiment. 2D peaks are elliptic with different "diagonal" and "antidiagonal" linewidths [Fig. 4(a)].[30] The intermediate regime may be observed at $\Lambda^{-1} < t_2 < k^{-1}$ when the bath loses memory [Fig. 4(b)], and the 2D peaks become symmetric. For long times $k_d t_2 \gg 1$ we see cross peaks induced by chemical exchange. Note the circular contours of Fig. 4(c), compared to the starlike contours for fast fluctuations (Fig. 3). These may be understood by noting that the product of two Gaussians (which represent the linear line shape for the slow case) is rotationally invariant, unlike the Lorentzian line shapes in the fast limit.

Figure 5 shows the $\mathbf{k}_\mathrm{I}$ and $\mathbf{k}_\mathrm{II}$ signals [Eqs. (8) and (9)]. The $\mathbf{k}_\mathrm{I}$ contribution dominates at short times, and shows effective rephasing (photon echo). The 2D IR spectrum is similar to the dominant $\mathbf{k}_\mathrm{I}$ contribution [see Fig. 4(a)]. For longer $t_2 \gg \Lambda^{-1}$ (right panels), the $\mathbf{k}_\mathrm{I}$ and $\mathbf{k}_\mathrm{II}$ contributions become comparable and S_A is symmetric (see Fig. 4).

We next explore some more general cases. First we take $\Delta_2 \neq 0$. The overtone peaks may now have different widths along ω_3 and ω_1. Overtone photon echoes are expected at $\Omega_2 t_1 = (\Omega_2 + \Delta_2) t_3$. Note that we have a slow bath ($\Lambda < \Omega_2$) for the eg and a fast bath for the ef transition ($\Lambda > \Omega_2 + \Delta_2$). These line shapes are shown in Fig. 6.

The inclusion of Ω_3 does not require additional numerical effort. This parameter allows the u and d peaks to have different widths due to spectral diffusion. To demonstrate these effects and relate them to the recent experiments[5] we have simulated the spectral diffusion using a single overdamped Brownian oscillator coordinate allowing a different width for u and d peaks. We used the splitting $2\Delta_0 = 34\ \mathrm{cm}^{-1}$ (i.e., $\sim 1.01\ \mathrm{ps}^{-1}$) and the exchange rates $k_u = 0.1\ \mathrm{ps}^{-1}$ and $k_d = 0.125\ \mathrm{ps}^{-1}$ as determined in Ref. 5 from the cross peak growth. Three regimes similar to those of Fig. 4 were observed[5] suggesting that the bath is not fast. The intermediate regime, where the memory of the Brownian oscillator coordinate is lost (circular line shape) but the cross peaks are still weak, was found on the 2 ps time scale. We thus assumed for the relaxation rate $\Lambda \sim 0.4\ \mathrm{ps}^{-1}$. Knowing Λ, Ω_1 and Ω_3 are connected to the peak linewidth in linear spectra and can be estimated using the Pade approximant of a two-level system.[25,31] We have simulated the absorption spectra in Fig. 7 and found line shapes similar to experiment for $\Omega_2 = 0.33\ \mathrm{ps}^{-1}$ and $\Omega_3 = -0.07\ \mathrm{ps}^{-1}$. This completely determines the model for 2D IR spectroscopy (neglecting dynamics in the overtone), we have no additional free param-

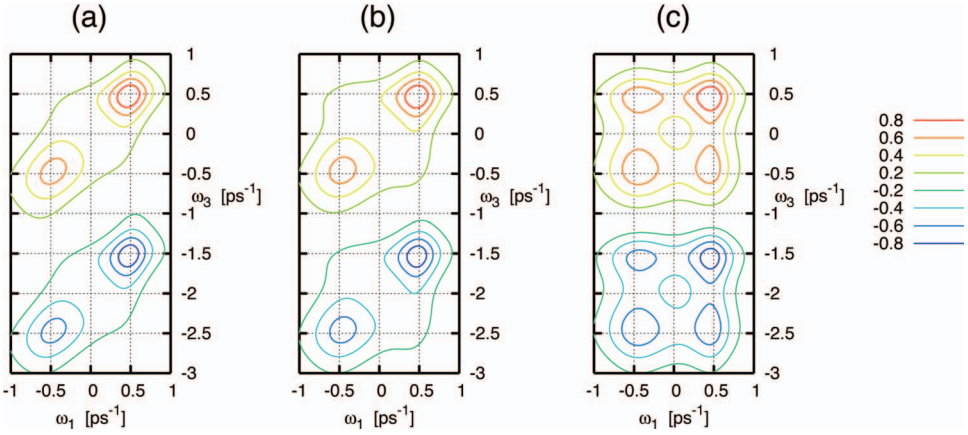

FIG. 8. (Color) The 2D signal S_A [Eq. (10)] for the same parameters of Fig. 7 at various time delays. (a) $t_2 = 0$, (b) $t_2 = 2$ ps, and (c) $t_2 = 10$ ps. These spectra closely resemble the experimental results of Ref. 5.

eter. The predicted 2D IR line shapes shown in Fig. 8 are in qualitative agreement with experiment. We reproduce all three regimes, rephasing elliptic shapes, the relaxed Brownian oscillator with circular shape, and chemical exchange cross peaks at the proper time scales. The peaks have also the correct relative intensity (the lower frequency peak is weaker but broader).

In conclusion, we have demonstrated that the SLE may be used to model chemical exchange in 2D IR spectroscopy. Spectral diffusion may not be accounted for by simply adding dephasing rates, when its time scale may be observed in experiment. Its proper description must be combined with the two-state jump which describe chemical exchange. The high temperature overdamped Brownian oscillator model for spectral diffusion with arbitrary fluctuation time scale reproduces all the regimes observed in recent experiments.[5]

In contrast with calculations based on the cumulant expansions at finite temperatures[18,25,32] our high temperature bath does not respond to the state of system, and its evolution in the ground and excited states is same.[25,37] This is why $R_i=R_{iii}$ and $R_{ii}=R_{iv}$. This may limit the applicability of the SLE model when signatures of the vibrational Stokes shift are observed in 2D signals. However, the Stokes shift is often negligible in the infrared, and the chemical exchange rates do not change with the vibrational state of molecule.[7] This limitation may be overcome by introducing a vibrational state dependent stochastic bath.[38,39] The lack of phase factors during the t_2 interval reduces the dynamics to classical level and allows large scale molecular-dynamics (MD) simulations of environmental dynamics.

ACKNOWLEDGMENTS

The support of NSF (Grant No. CHE-0446555) and NIH (Grant No. 2RO1GM59230-05) is gratefully acknowledged. One of the authors (F.Š.) is also supported by the Ministry of Education, Youth and Sports of the Czech Republic (Project No. MSM 0021620835).

APPENDIX A: THE ABSORPTION LINE SHAPE

The linear response function is given by[25]

$$S^{(1)}(t_1)=\theta(t_1)\frac{i}{\hbar}\langle\langle I|\mu^{(-)}\mathcal{G}(t_1)\mu^{(-)}|\rho(0)\rangle\rangle_{\mathcal{H}}.$$

We define the contribution

$$K(t_1)=\langle I|\mathcal{G}_{eg,eg}(t_1)|\rho(0)\rangle_{QS}.$$

This response function is connected to absorption line shape,

$$W(\omega_1)=\mu_{eg}^2\hbar^{-1}\,Re\int_0^\infty \exp(i\omega_1 t_1)K(t_1)dt_1. \tag{A1}$$

For the TSJ model ($\Omega_{2,3}=0$) the result of Kubo[19] is recovered,

$$W(\omega)=\frac{1}{(k_d+k_u)}\times\frac{4k_dk_u\Omega_1^2}{(\omega-\Omega_0-\Omega_1)^2+[(\omega-\Omega_0)(k_d+k_u)+\Omega_1(k_d-k_u)]^2}.$$

For the spectral diffusion model we set $\Omega_1=0$ and the linear response function is given by the second order cumulant expression [see Eq. (C6)].

$$K(t_1)=\exp(-g_{ee}(t_1)).$$

APPENDIX B: RESPONSE FUNCTIONS FOR TWO-STATE-JUMP SPIN DYNAMICS

In the frequency domain the Green's function [Eq. (18)] matrix elements are

$$\mathcal{G}_{\nu\nu',\nu_1\nu_1'}(\omega)=-[(i\omega+\hat{\mathcal{L}})^{-1}]_{\nu\nu',\nu_1\nu_1'}=\frac{-\delta_{\nu\nu_1}\delta_{\nu'\nu_1'}}{(\omega-\epsilon_0^{(\nu)}+\epsilon_0^{(\nu')})^2-(\epsilon_1^{(\nu)}+\epsilon_1^{(\nu')})^2+i(\omega-\epsilon_0^{(\nu)}+\epsilon_0^{(\nu')})(k_d+k_u)+i(\epsilon_1^{(\nu)}-\epsilon_1^{(\nu')})(k_d-k_u)}$$
$$\times\begin{pmatrix}k_u-i(\omega-\epsilon_0^{(\nu)}+\epsilon_0^{(\nu')}+\epsilon_1^{(\nu)}-\epsilon_1^{(\nu')}) & k_u\\ k_d & k_d-i(\omega-\epsilon_0^{(\nu)}+\epsilon_0^{(\nu')}-\epsilon_1^{(\nu)}+\epsilon_1^{(\nu')})\end{pmatrix}, \tag{B1}$$

R_i and R_{ii} [Eq. (6)] are given by

$$R_\alpha(\omega_3,t_2,\omega_1)=\frac{1}{(\omega\mp\Omega_0)^2-\Omega_1^2+i(\omega_1\mp\Omega_0)(k_d+k_u)\pm i\Omega_1(k_d-k_u)}$$
$$\times\frac{1}{(\omega_3-\Omega_0)^2-\Omega_1^2+i(\omega_3-\Omega_0)(k_d+k_u)+i\Omega_1(k_d-k_u)}\frac{1}{k_u+k_d}$$
$$\times\Big\{(k_u+k_d)^3-[(\omega_3-\Omega_0)(\omega_1\mp\Omega_0)\pm\Omega_1^2](k_u+k_d)+[(\omega_1\mp\Omega_0)\Omega_1\pm(\omega_3-\Omega_0)\Omega_1](k_d-k_u)$$
$$-i[(\omega_3-\Omega_0+\omega_1\mp\Omega_0)(k_u+k_d)^2-(\Omega_1\pm\Omega_1)(k_d^2-k_u^2)]\pm4\Omega_1^2k_uk_d\frac{1-\exp[-(k_d+k_u)t_2]}{k_d+k_u}\Big\},$$

where the upper (lower) sign in for R_i (R_{ii}). Since the evolution in the excited $|ee\rangle\rangle$ and in the ground $|gg\rangle\rangle$ state is the same for stochastic jumps (where the bath is not affected by the system) we have

$$R_{iii}(\omega_3,t_2,\omega_1)=R_i(\omega_3,t_2,\omega_1),\quad R_{iv}(\omega_3,t_2,\omega_1)=R_{ii}(\omega_3,t_2,\omega_1). \tag{B2}$$

We further have for R_v and R_{vi},

$$\begin{aligned}R_\alpha(\omega_3,t_2,\omega_1)=&-\frac{1}{(\omega_1\mp\Omega_0)^2-\Omega_1^2+i(\omega_1\mp\Omega_0)(k_d+k_u)\pm i\Omega_1(k_d-k_u)}\\&\times\frac{1}{(\omega_3-\Omega_0-\Delta_0)^2-(\Omega_1+\Delta_1)^2+i(\omega_3-\Omega_1-\Delta_1)(k_d+k_u)+i(\Omega_1+\Delta_1)(k_d-k_u)}\frac{1}{k_u+k_d}\\&\times\Big\{(k_u+k_d)^3-[(\omega_3-\Omega_0-\Delta_0)(\omega_1\mp\Omega_0)\pm(\Omega_1+\Delta_1)\Omega_1](k_u+k_d)+[(\omega_1\mp\Omega_1)(\Omega_1+\Delta_1)\pm(\omega_3-\Omega_0-\Delta_0)\Omega_1]\\&\times(k_d-k_u)-i[(\omega_3-\Omega_0-\Delta_0+\omega_1\mp\Omega_0)(k_u+k_d)^2-(\Omega_1+\Delta_1\pm\Omega_1)(k_d^2-k_u^2)]\\&\pm4(\Omega_1(\Omega_1+\Delta_1)\ k_uk_d\frac{1-\exp[-(k_d+k_u)t_2]}{k_d+k_u}\Big\},\end{aligned}$$

where the upper (lower) sign is for R_v (R_{vi}).

1. High temperature spin dynamics

In the high temperature limit we set $k_u=k_d\equiv k$. We first analyze the R_i and R_{ii} contributions. Here

$$\mathcal{G}_{eg,eg}(t)=e^{-(k+i\Omega_0)t}\begin{pmatrix}\cosh(\eta t)-\dfrac{i\Omega_1}{\eta}\sinh(\eta t) & \dfrac{k}{\eta}\sinh(\eta t)\\ \dfrac{k}{\eta}\sinh(\eta t) & \cosh(\eta t)+\dfrac{i\Omega_1}{\eta}\sinh(\eta t)\end{pmatrix}, \tag{B3}$$

and

$$\mathcal{G}_{ge,ge}(t)=\mathcal{G}^*_{eg,eg}(t),$$

where $\eta=\sqrt{k^2-\Omega_1^2}$. When $\Omega_1>k$ we use analytic continuation [e.g., $\cosh(ix)=\cos x$ and $\sinh(ix)=i\sin x$] and after some algebra we get for $\alpha=i,ii$,[21]

$$\begin{aligned}R_\alpha(t_3,t_2,t_1)=&\frac{e^{-k(t_1+t_3)}e^{-i\Omega(t_3\pm t_1)}}{2}\left[\left(1+\frac{k^2}{\eta^2}\right)\cosh[\eta(t_1+t_3)]+\left(1-\frac{k^2}{\eta^2}\right)\cosh[\eta(t_1-t_3)]+\frac{2k}{\eta}\sinh[\eta(t_1+t_3)]\right]\\&\mp e^{-k(t_1+2t_2+t_3)}e^{-i\Omega(t_3\pm t_1)}\frac{\omega_0^2}{2\eta^2}[\cosh[\eta(t_1+t_3)]-\cosh[\eta(t_1-t_3)]],\end{aligned} \tag{B4}$$

where the upper (lower) sign stands for R_i (R_{ii}). Equation (7) then gives

$$\begin{aligned}R_\alpha(\omega_3,t_2,\omega_1)=&\frac{1}{(\omega_1\mp\Omega_0)^2-\Omega_1^2+2i(\omega_1\mp\Omega_0)k}\frac{1}{(\omega_3-\Omega_0)^2-\Omega_1^2+2i(\omega_3-\Omega_0)k}\\&\times\{4k^2-(\omega_3-\Omega_0)(\omega_1\mp\Omega_0)\mp\Omega_1^2-2i(\omega_3-\Omega_0+\omega_1\mp\Omega_0)k\pm\Omega_1^2[1-\exp(-2kt_2)]\}.\end{aligned}$$

We further have $R_{iii}=R_i$ and $R_{iv}=R_{ii}$. For $\alpha=v,vi$ we get

$$\begin{aligned}R_\alpha(\omega_3,t_2,\omega_1)=&\frac{1}{(\omega_1\mp\Omega_0)^2-\Omega_1^2+2i(\omega_1\mp\Omega_0)k}\frac{1}{(\omega_3-\Omega_0-\Delta_0)^2-(\Omega_1+\Delta_1)^2+2i(\omega_3-\Omega_1-\Delta_1)k}\{4k^2-[(\omega_3-\Omega_0-\Delta_0)\\&\times(\omega_1\mp\Omega_0)\pm(\Omega_1+\Delta_1)\Omega_1]-2i[(\omega_3-\Omega_0-\Delta_0+\omega_1\mp\Omega_0)k]\pm\Omega_1(\Omega_1+\Delta_1)(1-\exp[-2kt_2])\},\end{aligned}$$

where the upper (lower) sign corresponds to R_v (R_{vi}).

2. Slow spin dynamics

When $\Omega_1\gg k_u,k_d$ no spin jumps occur during the t_1 and t_3 intervals. Then

$$\mathcal{G}_{\nu\nu',\nu_1\nu_1'}(\omega)=\delta_{\nu\nu_1}\delta_{\nu'\nu_1'}\begin{pmatrix}k_d+i(\epsilon_0^{(\nu)}-\epsilon_0^{(\nu')}+\epsilon_1^{(\nu)}-\epsilon_1^{(\nu')}-\omega) & 0\\ 0 & k_u+i(\epsilon_0^{(\nu)}-\epsilon_0^{(\nu')}-\epsilon_1^{(\nu)}+\epsilon_1^{(\nu')}-\omega)\end{pmatrix}^{-1}.$$

The Green's function for t_2 is still given by Eq. (19).

In the vicinity of the peaks [Fig. 2(a)] at, e.g., $\omega_1\approx\Omega_0+\Omega_1$, and $\omega_3\approx\Omega_0-\Omega_1$, we have

$$R_i(\omega_3,0,\omega_1)\propto\frac{1}{k_u-i(\omega_1-\Omega_0-\Omega_1)}\frac{1}{k_d-i(\omega_3-\Omega_0+\Omega_1)}$$
$$=\frac{k_dk_u-(\omega_1-\Omega_0-\Omega_1)(\omega_3-\Omega_0+\Omega_1)+i[k_d(\omega_1-\Omega_0-\Omega_1)+k_u(\omega_3-\Omega_0+\Omega_1)]}{(k_u^2+(\omega_1-\Omega_0-\Omega_1)^2)(k_d^2+(\omega_3-\Omega_0+\Omega_1)^2)},$$

$$R_{ii}(\omega_3,0,\omega_1)\propto\frac{1}{k_u-i(\omega_1+\Omega_0+\Omega_1)}\frac{1}{k_d-i(\omega_3-\Omega_0+\Omega_1)}$$
$$=\frac{k_dk_u-(\omega_1+\Omega_0+\Omega_1)(\omega_3-\Omega_0+\Omega_1)+i[k_d(\omega_1+\Omega_0+\Omega_1)+k_u(\omega_3-\Omega_0+\Omega_1)]}{(k_u^2+(\omega_1+\Omega_0+\Omega_1)^2)(k_d^2+(\omega_3-\Omega_0+\Omega_1)^2)}.$$

In the absorptive signal [Eq. (10)] the dispersive parts (the second term in nominator) cancel out and the signal is given by simple Lorentzian linear response peaks,

$$S_A(\omega_3,0,\omega_1)$$
$$\propto\frac{4\mu_{eg}^4k_dk_u}{\hbar^3(k_u^2+(\omega_1-\Omega_0-\Omega_1)^2)(k_d^2+(\omega_3-\Omega_0+\Omega_1)^2)}$$
$$=\hbar^{-1}W(\omega_1)W(\omega_3). \tag{B5}$$

3. Fast spin fluctuations; motional narrowing

In the $k_u,k_d\gg\Omega_1$ limit we get

$$\mathcal{G}_{eg,eg}(\omega)=\frac{-1}{(\omega-\Omega_0)^2+i(\omega-\Omega_0)(k_d+k_u)}\times\begin{pmatrix}k_u-i(\omega-\Omega_0) & k_u\\ k_d & k_d-i(\omega-\Omega_0)\end{pmatrix},$$

$$\mathcal{G}_{ge,ge}(\omega)=\mathcal{G}_{eg,eg}(-\omega)^*.$$

The line shapes are insensitive to t_2 delay one can set

$$\mathcal{G}_{ee,ee}(t_2)=\mathcal{G}_{gg,gg}(t_2)=\frac{1}{k_u+k_d}\begin{pmatrix}k_u & k_u\\ k_d & k_d\end{pmatrix}=\frac{1}{k_u+k_d}\begin{pmatrix}k_u\\ k_d\end{pmatrix}(1\ 1).$$

The response functions may now be factorized into products of the linear response functions [Eq. (11)].

APPENDIX C: THE CUMULANT EXPANSION FOR THE SPECTRAL DIFFUSION MODEL

Neglecting spin dynamics by setting $\Delta_1=\Delta_3=0$ and $\Omega_1=\Omega_3=0$, the response functions may be calculated by the second order cumulant expansion[25,33] which represents stochastic Gaussian fluctuations. The response function may then be expressed in terms of the following four-point correlation functions:[34]

$$F_1(\tau_4,\tau_3,\tau_2,\tau_1)\equiv\langle B(\tau_4)B^\dagger(\tau_3)B(\tau_2)B^\dagger(\tau_1)\rangle,$$
$$F_2(\tau_4,\tau_3,\tau_2,\tau_1)\equiv\langle B(\tau_4)B(\tau_3)B^\dagger(\tau_2)B^\dagger(\tau_1)\rangle/2. \tag{C1}$$

We then have[34–36]

$$R_i(t_3,t_2,t_1)=F_1(t_1,t_1+t_2,t_1+t_2+t_3,0),$$
$$R_{ii}(t_3,t_2,t_1)=F_1(0,t_1+t_2,t_1+t_2+t_3,t_1),$$
$$R_{iii}(t_3,t_2,t_1)=F_1(t_1+t_2+t_3,t_1+t_2,t_1,0),$$
$$R_{iv}(t_3,t_2,t_1)=F_1(0,t_1,t_1+t_2+t_3,t_1+t_2),$$
$$R_v(t_3,t_2,t_1)=F_2(t_1,t_1+t_2+t_3,t_1+t_2,0),$$
$$R_{vi}(t_3,t_2,t_1)=F_2(0,t_1+t_2+t_3,t_1+t_2,t_1). \tag{C2}$$

Here

$$F_1(\tau_4,\tau_3,\tau_2,\tau_1)=\exp[i(-\Omega_0\tau_4+\Omega_0\tau_3-\Omega_0\tau_2+\Omega_0\tau_1)-f_1(\tau_4,\tau_3,\tau_2,\tau_1)], \tag{C3}$$

with

$$f_1(\tau_1,\tau_2,\tau_3,\tau_4)=g_{ee}(t_{21})+g_{ee}(t_{43})+g_{ee}(t_{32})+g_{ee}(t_{41})-g_{ee}(t_{31})-g_{ee}(t_{42}),$$

where $t_{ij}\equiv\tau_i-\tau_j$ and

$$F_2(\tau_4,\tau_3,\tau_2,\tau_1)=\exp[i(\Omega_0\tau_4-(\Omega_0+\Delta_0)\tau_3+(\Omega_0+\Delta_0)\tau_2+\Omega_0\tau_1)-f_2(\tau_4,\tau_3,\tau_2,\tau_1)], \tag{C4}$$

with

$$f_2(\tau_1,\tau_2,\tau_3,\tau_4)=g_{ee}(t_{21})+g_{ff}(t_{32})+g_{ee}(t_{43})-g_{ef}(t_{21})-g_{ef}(t_{32})+g_{ef}(t_{31})+g_{ee}(t_{32})+g_{ee}(t_{41})-g_{ee}(t_{31})-g_{ee}(t_{42})-g_{fe}(t_{32})-g_{fe}(t_{43})+g_{fe}(t_{42}). \tag{C5}$$

g_{ab} are the line broadening functions,[25,34]

$$g_{ee}(t)=\Omega_2^2[\exp(-\Lambda t)+\Lambda t-1],$$
$$g_{ef}(t)=(\Omega_2+\Delta_2)\Omega_2[\exp(-\Lambda t)+\Lambda t-1], \tag{C6}$$
$$g_{ff}(t)=(\Omega_2+\Delta_2)^2[\exp(-\Lambda t)+\Lambda t-1].$$

Note that $R_i=R_{iii}$ and $R_{ii}=R_{iv}$ as expected for stochastic models of frequency fluctuations.

APPENDIX D: SPECTRUM OF THE FOKKER-PLANCK EQUATION

The eigenvectors of the Fokker-Planck operator [Eq. (20)] with eigenvalue $-\alpha\Lambda$ are given by[27]

$$|\alpha\rangle_Q = \frac{\exp[-(Q^2/2)]}{2^n\sqrt{2\pi}n!}H_\alpha\left(\frac{Q}{\sqrt{2}}\right), \quad \alpha = 0,1,2,\ldots, \tag{D1}$$

where H_α is the Hermite polynomial,

$$H_\alpha(x) = (-1)^n e^{x^2}\frac{d^\alpha}{dx^\alpha}e^{-x^2}.$$

The matrix representation of bath densities and evolution matrices refer to to the basis $\{|\alpha\rangle_Q\}$. The matrix elements of L_Q are

$$(L_Q)_{\beta,\alpha} = -\alpha\Lambda\delta_{\alpha,\beta}. \tag{D2}$$

We use the recurrence relation,

$$QH_\alpha(Q) = \frac{H_{\alpha+1}(Q)}{2} + nH_{\alpha-1}(Q). \tag{D3}$$

The Q coordinate is then represented by the tridiagonal matrix [Eq. (D4)].

$$[Q]_{\beta\alpha} = \beta\sqrt{2}\delta_{\beta,\alpha+1} + \frac{1}{\sqrt{2}}\delta_{\beta,\alpha-1}. \tag{D4}$$

APPENDIX E: MATRIX CONTINUED-FRACTION SOLUTION OF THE FOKKER-PLANCK EQUATION

The complete Liouville superoperator is an 18×18 matrix in the joint vibrational and spin space. The Q variable is tridiagonal in the Fokker-Planck eigenbasis and the complete Liouvillean may be thus arranged in the tridiagonal block structure in the Brownian coordinate variable,

$$i\omega + \hat{\mathcal{L}} = \begin{pmatrix} \mathcal{Q}_0 & \mathcal{Q}_0^+ & 0 & 0 & \cdots & \cdots \\ \mathcal{Q}_1^- & \mathcal{Q}_1 & \mathcal{Q}_1^+ & 0 & \cdots & \cdots \\ \cdots & \cdots & \cdots & \cdots & \cdots & \cdots \\ 0 & \cdots & \mathcal{Q}_n^- & \mathcal{Q}_n & \mathcal{Q}_n^+ & \cdots \\ \cdots & \cdots & \cdots & \cdots & \cdots & \cdots \end{pmatrix}. \tag{E1}$$

For Eq. (22) the blocks are

$$\mathcal{Q}_n = i\omega + \hat{L}_S + \hat{\mathcal{L}}_S - n\Lambda\hat{1},$$

$$\mathcal{Q}_n^- = \frac{1}{\sqrt{2}}\hat{\mathcal{L}}_{QS},$$

$$\mathcal{Q}_n^+ = \sqrt{2}(n+1)\hat{\mathcal{L}}_{QS}.$$

The SLE may be solved in the frequency domain using a matrix continued fraction.[17,27,29] The Green's function is given by the inverse [Eq. (24)] of the tridiagonal matrix Eq. (E1). Starting with

$$[i\omega + \hat{\mathcal{L}}]\mathcal{G}(\omega) = -\hat{1}.$$

For the off-diagonal $n\neq m$ elements we have

$$\mathcal{Q}_n^-\mathcal{G}_{n-1,m} + \mathcal{Q}_n\mathcal{G}_{n,m} + \mathcal{Q}_n^+\mathcal{G}_{n+1,m} = 0. \tag{E2}$$

The diagonal $n=m$ elements are

$$\mathcal{Q}_n^-\mathcal{G}_{n-1,n} + \mathcal{Q}_n\mathcal{G}_{n,n} + \mathcal{Q}_n^+\mathcal{G}_{n+1,n} = -1. \tag{E3}$$

The recursion relation Eq. (E2) is independent of the index m. Consequently we can introduce the matrices $\mathcal{S}^+$ and $\mathcal{S}^-$,

$$\mathcal{G}_{n\pm1,b} = \mathcal{S}_n^\pm\mathcal{G}_{n,m}. \tag{E4}$$

Using Eq. (E2) these matrices may be solved iteratively.

$$S_n^\pm = \frac{-1}{\mathcal{Q}_{n\pm1} + \mathcal{Q}_{n\pm1}^\pm\mathcal{S}_{n\pm1}^\pm}\mathcal{Q}_{n\pm1}^\mp. \tag{E5}$$

Combined with Eq. (E3) we obtain for the diagonal terms,

$$\mathcal{G}_{n,n} = \frac{-1}{\mathcal{Q}_n^-\mathcal{S}_n^- + \mathcal{Q}_n + \mathcal{Q}_n^+\mathcal{S}_n^+}, \tag{E6}$$

while the off-diagonal $\mathcal{G}(\omega)_{nm}$ are obtained from Eqs. (E5) and (E4). For $n>m$,

$$\mathcal{G}_{n,m}(\omega) = \mathcal{S}_{n-1}^+(\omega)\mathcal{S}_{n-2}^+(\omega)\cdots\mathcal{S}_m^+(\omega)\mathcal{G}_{m,m}(\omega), \tag{E7}$$

and for $n<m$,

$$\mathcal{G}_{n,m}(\omega) = \mathcal{S}_{n+1}^-(\omega)\mathcal{S}_{n+2}^-(\omega)\cdots\mathcal{S}_m^-(\omega)\mathcal{G}_{m,m}(\omega). \tag{E8}$$

The full Green's function $\mathcal{G}(\omega)$ can be calculated by using Eq. (E5) to find the connection matrices $\mathcal{S}^\pm$. We note that $\mathcal{S}_0^-$ is zero and truncate the recurrence relation for $\mathcal{S}^+$ at some level n by setting $\mathcal{S}_n^+$ equal to zero. The matrix elements $\mathcal{G}(\omega)_{mm}$ can then be obtained using Eq. (E6). All other matrix elements $\mathcal{G}(\omega)_{nm}$ are calculated from Eq. (E4).

[1] R. R. Ernst, G. Bodenhausen, and A. Wokaun, *Principles of Nuclear Magnetic Resonance in One and Two Dimensions* (Oxford University Press, New York, 1987).
[2] B. H. Meier and R. R. Ernst, J. Am. Chem. Soc. **101**, 6441 (1979).
[3] D. Gamliel and H. Levanon, *Stochastic Processes in Magnetic Resonance* (World Scientific, Singapore, 1995).
[4] R. Kubo, in *Fluctuation, Relaxation and Resonance in Magnetic Systems*, edited by D. ter Haar (Oliver and Boyd, Edingburgh, 1962), p. 23.
[5] J. Zheng, K. Kwak, J. Asbury, X. Chen, I. R. Piletic, and M. D. Fayer, Science **309**, 1338 (2005).
[6] J. Asbury, T. Steinel, and M. D. Fayer, J. Lumin. **107**, 271 (2004).
[7] Y. S. Kim and R. M. Hochstrasser, Proc. Natl. Acad. Sci. U.S.A. **102**, 1185 (2005).
[8] S. Mukamel, Annu. Rev. Phys. Chem. **51**, 691 (2000).
[9] D. M. Jonas, Annu. Rev. Phys. Chem. **54**, 425 (2003).
[10] Chem. Phys. **266**, 2 (2001), special issue on multidimensional spectroscopy, edited by S. Mukamel and R. M. Hochstrasser.
[11] Ch. Scheurer and S. Mukamel, J. Chem. Phys. **115**, 4989 (2001).
[12] M. Khalil, N. Demirdöven, and A. Tokmakoff, Phys. Rev. Lett. **90**, 047401 (2003).
[13] N. G. van Kampen, *Stochastic Processes in Physics and Chemistry* (North Holland, Amsterdam, 1992).
[14] S. N. Vinogradov and R. H. Linell, *Hydrogen Bonding* (Van Nostrand Reinhold, New York, 1971).
[15] *The Hydrogen Bond: Recent Developments in Theory and Experiments*, edited by P. Schuster, G. Zundel, and C. Sandorfy (North-Holland, Amsterdam, 1976).
[16] *Ultrafast Hydrogen Bonding Dynamics and Proton Transfer Processes in the Condenced Phase*, edited by T. Elsaesser and H. J. Bakker (Kluwer Academic, Dordrecht, 2002).
[17] T. L. C. Jansen, W. Zhuang, and S. Mukamel, J. Chem. Phys. **121**, 10577 (2004).
[18] T. L. C. Jansen, T. Hayashi, W. Zhuang, and S. Mukamel, J. Chem. Phys. **123**, 114504 (2005).

[19] R. Kubo, J. Math. Phys. **4**, 174 (1963).
[20] P. W. Anderson, B. I. Halperin, and C. M. Varma, Philos. Mag. **25**, 1 (1971).
[21] Y. Zhao, V. Chernyak, and S. Mukamel, J. Phys. Chem. A **102**, 6614 (1998).
[22] F. Šanda and S. Mukamel, Phys. Rev. E **73**, 011108 (2006).
[23] A. O. Caldeira and A. J. Leggett, Physica A **121**, 587 (1983).
[24] C. Cohen-Tanoudji, J. Dupon-Roc, and G. Gryndberg, *Atom Photon Interaction* (Wiley, New York, 1957).
[25] S. Mukamel, *Principles of Nonlinear Optical Spectroscopy* (Oxford University Press, New York, 1995).
[26] R. Kubo, M. Toda, and N. Hashitsume, *Statistical Physics II* (Springer, Berlin, 1995).
[27] H. Risken, *The Fokker-Planck Equation* (Springer, Berlin, 1989).
[28] Y. Tanimura and T. Steffen, J. Phys. Soc. Jpn. **69**, 4095 (2000).
[29] Y. Tanimura and R. Kubo, J. Phys. Soc. Jpn. **58**, 101 (1989).
[30] K. Okomura, A. Tokmakoff, and Y. Tanimura, Chem. Phys. Lett. **314**, 488 (1999).
[31] Y. J. Yan and S. Mukamel, J. Chem. Phys. **89**, 5160 (1988).
[32] J. J. Markham, Rev. Mod. Phys. **31**, 965 (1959).
[33] S. Mukamel, Phys. Rev. A **28**, 3480 (1983).
[34] D. Abramavicius and S. Mukamel, Chem. Rev. (Washington, D.C.) **104**, 2073 (2004).
[35] R. Venkatramani and S. Mukamel, J. Chem. Phys. **117**, 11089 (2002).
[36] T. Meier, V. Chernyak, and S. Mukamel, J. Chem. Phys. **107**, 8759 (1997).
[37] F. Šanda and S. Mukamel, Phys. Rev. A **71**, 033807 (2005).
[38] A. Garg, J. N. Onuchic, and V. Ambegaokar, J. Chem. Phys. **83**, 4491 (1985).
[39] D. Zusman, Chem. Phys. **49**, 295 (1980).